

# Comprehensive benchmarking of large language models for RNA secondary structure prediction

L.I. Zablocki, L.A. Bugnon, M. Gerard, L. Di Persia, G. Stegmayer, D.H. Milone

Research Institute for Signals, Systems and Computational Intelligence  
sinc(i), FICH-UNL, CONICET, Santa Fe, Argentina

## Abstract

In recent years, inspired by the success of large language models (LLM) for DNA and proteins, several LLM for RNA have also been developed. These models take massive RNA datasets as inputs and learn, in a self-supervised way, how to represent each RNA base with a semantically rich numerical vector. This is done under the hypothesis that obtaining high-quality RNA representations can enhance data-costly downstream tasks, such as the fundamental RNA secondary structure prediction problem. However, existing RNA-LLM have not been evaluated for this task in a unified experimental setup. Since they are pre-trained models, assessment of their generalization capabilities on new structures is a crucial aspect. Nonetheless, this has been just partially addressed in literature. In this work we present a comprehensive experimental and comparative analysis of pre-trained RNA-LLM that have been recently proposed. We evaluate the use of these representations for the secondary structure prediction task with a common deep learning architecture. The RNA-LLM were assessed with increasing generalization difficulty on benchmark datasets. Results showed that two LLM clearly outperform the other models, and revealed significant challenges for generalization in low-homology scenarios. Moreover, in this study we provide curated benchmark datasets of increasing complexity and a unified experimental setup for this scientific endeavor.

Availability: The source code to reproduce all the experiments and results can be found in: <https://github.com/sinc-lab/rna-llm-folding>

## Introduction

Ribonucleic acid (RNA) plays a crucial role in many fundamental biological processes, such as gene expression, cell signaling, and post-transcriptional regulation [26, 72]. As in proteins, RNAs function and interaction with other molecules are deeply related to their structure. For example, determining RNA structure is essential for RNA-based therapeutics such as mRNA vaccines [42]. Among all RNA transcripts, only 5% is responsible for protein coding. At the same time, a very large remaining portion is non-coding RNA (ncRNA) [9], which in many cases adopt specific structures to perform important biological functions [8, 3]. Experimental results show that, to some degree, sequence determines the secondary structure, and thus, their function [40, 20, 67]. Therefore, the long-established and yet unresolved RNA secondary structure prediction is a major challenge in computational biology today [6, 7].

During many years, experimental molecular structure technologies like nuclear magnetic resonance, X-ray crystallography and cryogenic electron microscopy have produced several RNA structures [25, 58]. However, despite the large number of ncRNA sequences available, most of their structures and functions remain still unknown [74]. At the same time that large amounts of unlabeled RNA sequence data were produced by high-throughput sequencing technologies, pre-trained RNA language models have started to be used for modeling the semantic space of RNA sequences, intending to facilitate its understanding. Motivated by the success of large language models (LLM) in proteins [39, 45, 24, 4, 2, 47, 17, 38] and DNA [32], several RNA LLM have recently appeared [1, 44, 11, 71, 78, 75, 70] with the potential to be used for improving several important RNA-related tasks, among which one of the most relevant is RNA secondary structure prediction.

RNA-LLM attempt to effectively embed RNA bases using deep representation learning, in particular the one developed in the field of natural language processing [24, 47]. Most RNA-LLM are based on bidirectional encoder representations from transformers (BERT), which was designed to generate context-sensitive distributed test token (word) representations [15]. The relevance of LLM for transfer learning from sequences to downstream tasks have been analyzed in detail for proteins [66, 31, 68]. In the case of RNA, the hypothesis is that LLM representation of nucleotide composition and sequence motifs can help characterize the structure and function of a sequence, analogously to how the meaning of a sentence is determined by the grammatical structure of natural language. Thus, word embedding techniques for natural language have been applied to bases for RNA sequences, obtaining a wide variety of BERT-based architectures trained on different databases. However, in spite that some theoretical reviews on the applications and utility of LLM in bioinformatics have recently appeared [32, 63, 43], to the best of our knowledge all the available RNA-LLM have not yet been comparatively evaluated for the secondary structure prediction task, considering a fair experimental setup, with the same datasets and structure prediction model. Since LLM are pre-trained models, it is important to analyze how they were trained to assess generalization capabilities on new sequences/structures, considering homology-aware partitions and cross-family predictions.

Table 1 RNA large language models included in this study.

RNA-LLM	Year	Emb. Dim.	Pre-train seqs.	Databases	Architecture (layers)	Parameters	Repository
RNABERT [1]	2022	120	76,237	RNAcentral	Transformer (6)	509,896	
Pre-training with masked language modeling (MLM)[16] masking 15% random bases and predicting from neighboring bases, with data augmentation taking 10 copies of each ncRNA and applying 10 different mask patterns. Structural alignment learning (SAL) pre-training task based on seed alignment for each RNA family with Rfam. Token embedding randomly generated 120 dimensions RNA bases. Positional embedding for each base in the sequence. Stack of transformers with multi-head self-attention and feed-forward neural network. Softmax output layer. Cross-entropy loss function.							
RNA-FM [11]	2022	640	23,700,000	RNAcentral	Transformer (12)	~100,000,000	
Pre-training with MLM and 15% random masking. Based on BERT original architecture. Transformer encoder blocks, with multi-head self-attention modules and feed-forward layers. Softmax output layer. Cross-entropy loss function.							
RNA-MSM [78]	2024	768	3,087,138	Rfam	Transformer (12)	~96,000,000	
Multiple sequence alignment (MSA) inspired by AlphaFold2 [27]. Pre-training with MLM and 20% random masking. Homology search and MSA of training sequences with RNAm3 database [12] as augmented input. Two modules: embedding and MSA transformer. Initial embedding layer and two learnable position-embedding layers. Stack of MSA transformer blocks with a residue and sequence attention layer followed by a feed-forward layer with GELU activation functions. Cross-entropy loss function.							
ERNIE-RNA [75]	2024	768	20,400,000	RNAcentral	Transformer (12)	86,000,000	
Pre-training with MLM and 15% random masking. Based on the Enhanced Representation through Knowledge Integration (ERNIE) framework [60]. Modified BERT that incorporates base-pairing informed attention bias when calculating attention. From the second layer onward, the bias of each layer is determined by the attention map of the previous layer. Transformer blocks with attention heads followed by a feed-forward layer. Cross-entropy loss function.							
RNAErnie [70]	2024	768	~23,000,000	RNAcentral	Transformer (12)	~105,000,000	
Pre-training with MLM and 15% random masking. Motif-aware additional pre-training strategy involving motif-level random masking from motif databases [30], and random subsequence masking. Built upon the ERNIE framework. Transformer blocks followed by a feed-forward layer. Cross-entropy loss function.							
RiNALMo [44]	2024	1280	~36,000,000	RNAcentral + Rfam + Ensembl	Transformer (33)	~650,000,000	
Pre-training with MLM and 15% random masking and FlashAttention-2 [14]. BERT-style encoder-only transformer. Position encoded using rotary positional embedding [59]. Each block comprises a multi-head attention of 20 heads. Feed-forward network with two linear layers and SwiGLU activation functions [53]. Residual connections with layer normalization to stabilize training. Cross-entropy loss function.							

In this work, we provide a comprehensive experimental comparison of the latest pretrained RNA-LLM, using a unified and consistent experimental setup. It offers an independent, third-party assessment following the best practice guidelines for bias-free evaluations in the community [77]. We provide a description of each model, together with an experimental testing in four benchmarks of increasing complexity, with the corresponding source code and datasets to ensure reproducibility, supporting the development and boosting of future improvements on RNA secondary structure prediction based on LLM.

## RNA large language models evaluated

In the last three years, a number of RNA-LLM have appeared in literature. The following RNA-LLM (summarized in Table 1) were included in this study according to their availability as open source tools.

**RNABERT [1]:** For the pre-training of the masked language modeling (MLM)[16] task in this LLM, 76,237 human derived small ncRNAs from RNAcentral [62] were utilized. First, a token embedding randomly generates a 120-dimensional numerical vector that encodes the four RNA bases (A, C, G, U) and assigns the same vector to each base in the input RNA sequence. Second, the position embedding generates a 120-dimensional vector that encodes the position information of each base in the sequence. Third, the element-wise sum of token embedding and position embedding for each base in the input RNA sequence is fed to the Transformer layer. RNABERT architecture consists of a stack of 6 Transformers, each of which is composed of a multi-head self-attention mechanism followed by a feed-forward neural network. The weights of the last layer are trained by alternating between different tasks. The MLM task masks 15% of the bases randomly selected from the input RNA sequence and predicts the masked part using the neighboring bases, enabling a context sensitive embedding. The structural alignment learning (SAL) task is based on RNA structural alignment and aims to obtain closer embeddings for bases in the same column of reference alignment. The seed alignment for each family was downloaded from Rfam [28] as the reference structural alignment. The MLM task enables the position and context-sensitive embedding, and the SAL task enables the structural information embedding.

**RNA-FM [11]:** It is a 100 million parameter foundation model encoder based on the BERT original implementation and trained on 23.7 million unannotated ncRNAs from RNAcentral [62] database. Identical sequences were removed by applying CD-HIT [19] with a cut-off at 100%. The resulting dataset was used to train the foundation model in a self-supervised manner, reconstructing the input masked tokens as a pretext task. During pre-training under self-supervised training, around 15% of nucleotide tokens were randomly replaced with a special mask token. RNA-FM takes raw sequential tokens as input and embeds each nucleotide into a 640-dimensional vector. The architecture has 12 transformer encoder blocks as in BERT, which includes multi-head self-attention modules and feed-forward layers, with a final softmax layer to predict the output. The model was trained with MLM by predicting the original masked token with cross-entropy loss.

**RNA-MSM** [78]: Inspired by the success of AlphaFold2 [27] and the use of homologous sequences for the highly accurate prediction of protein structures, RNA-MSM is a multiple sequence alignment (MSA)-based RNA language model. It utilizes a set of homologous sequences that allows having a larger number of sequences for training. 4,069 RNA families were downloaded from Rfam 14.7, totaling 3,087,138 sequences. The RNACmap3 database [12] for homolog search and sequence alignment was employed. Rfam families containing RNA sequences with experimentally determined structures were excluded to minimize potential overfitting for downstream tasks such as structural inference. This led to a total of 3,932 Rfam families. Pre-training was based on MLM, with 20% random masking. The embedding module, with one initial embedding layer and two learnable position-embedding layers, encodes entries in the MSA separately. The architecture is made of a stack of MSA transformer blocks, each with a residue and sequence attention layer containing 12 heads with an embedding size of 768, followed by a feed-forward layer, which summarizes approximately 96 million parameters. The use of structural information associated with the sequences was not included during the LLM pre-training. To provide a fair comparison with the other RNA-LLM, a single-sequence version of this method was used. This way, the embedding obtained corresponds only to the input sequence.

**ERNIE-RNA** [75]: This RNA pre-trained language model is based on the Enhanced Representation through Knowledge Integration (ERNIE) framework [60] and a modified BERT that incorporates base-pairing restrictions to be used with RNA. For training the model, a 34 million ncRNA dataset from the RNACentral database was downloaded. After refining the vocabulary and removing redundant sequences, the final dataset consisted of 20.4 million RNA sequences. ERNIE-RNA was trained with MLM, which predicts the masked token with cross-entropy loss. The architecture has 12 transformer blocks, with 12 attention heads each. Every token in the input sequences is mapped to a 768-dimensional vector, resulting in 86 million parameters. The main hypothesis is that ERNIE-RNA can learn functional and structural information thanks to the use of attention maps during pre-training.

**RNAErnie** [70]: It is also built upon the Enhanced Representation through Knowledge Integration (ERNIE) framework [60], together with multilayer and multihead transformer blocks. Pre-training was done with a corpus of approximately 23 million sequences extracted from the RNACentral, and using self-supervised learning with multilevel random masking. The main difference with other works was the use of a motif-aware pre-training strategy involving motif-level and subsequence random masking, which can capture both subsequence and motif-level knowledge extracted from motif databases [30]. The architecture of RNAErnie shares the same architectural configuration as ERNIE 2.0 [61]: a 12-layer transformer with a hidden state embedding dimension of 768. A block first tokenizes RNA bases in the sequence and subsequently feeds them into the transformer. Given the embeddings for every token in the RNA sequence, the RNAErnie basic block transforms the series of token embeddings into a  $768 \times L$  embedding using trainable parameters and then outputs the embedding of the RNA sequence. The total number of trainable parameters in RNAErnie is approximately 105 million.

**RiNALMo** [44]: It is the largest RNA language model to date with 650 million parameters pre-trained on 36 million unique non-coding RNA sequences from the RNACentral [62] database augmented by Rfam [29], nt [52] and Ensembl [34]. To ensure diversity in each batch, the sequences were clustered with MMSeqs2 [57] into 17 million clusters, and then each batch contained a mixture of sequences sampled from different clusters. The architecture of RiNALMo is a BERT-style encoder-only Transformer [16]. Before passing to the Transformer, an RNA sequence is tokenized and represented as a 1280-dimensional vector. RiNALMo consists of 33 Transformer blocks, where each block comprises a multi-head attention and a feed-forward network. The position of the tokens is encoded using rotary positional embedding [59]. Each multi-head attention has 20 heads. To improve pre-training efficiency, FlashAttention-2 [14] is employed. In the feed-forward network, two linear layers are used together with SwiGLU activation function [53]. Among the transformer modules, there are residual connections with layer normalization to stabilize training.

## Materials and methods

### Data

The following datasets have been used in this study. For all datasets, sequences longer than 512 nucleotides were filtered to limit computational requirements [64]. That is, 512 nt is the top length in each dataset.

**ArchiveII dataset** [56]: The most widely used benchmark dataset for RNA folding methods, containing RNA structures from 9 RNA families: 5s (ribosomal RNAs), srp (signal recognition particle), tRNA (transfer RNA), tmRNA (transfer messenger RNA), RNaseP (Ribonuclease P), grp1 (Glycine-rich RNA-binding protein 1), 16s (ribosomal RNA), telomerase and 23s (ribosomal RNA). The total number of sequences is 3,864. This dataset is used in two training and testing split configurations. First, a random set of 5-fold partitions, following the original splits provided by the authors for the ArchiveII dataset [56]. We also perform a cross-family generalization analysis, training on all RNA families but one that is used as a test unseen family, and repeating for all families. That is, a leave-one-family-out strategy.

**bpRNA dataset** [54]: The same train and test sets as used in SPOT-RNA[54]. It is a non-redundant set of RNA sequences at 80% sequence-identity cutoff with CD-HIT-EST, with annotated secondary structure from bpRNA34 [19]. This filtered dataset of 13,419 RNAs is randomly divided into 10,814 RNAs for training (TR0), 1,300 for validation (VL0), and 1,305 for an independent test (TS0). In this dataset, each model was trained with TR0+VL0 and tested with TS0.

**bpRNA-new dataset** [54]: This dataset was derived from Rfam 14.2 [29], containing new RNA families different from the bpRNA dataset. This test dataset has 5,401 sequences and was built to assess cross-family model generalization.

This dataset is used as an additional test set for the models trained with the bpRNA dataset.

**PDB-RNA dataset** [50] The PDB sets TR1 (training), VL1 (validation) and TS1 (testing) are the same sets as in SPOT-RNA, prepared by downloading all the high-resolution ( $< 3.5\text{\AA}$ ) RNA X-ray structures from the PDB dataset on March 2, 2019. The numbers of structures for TR1, VL1 and TS1 are 120, 30 and 62, respectively, after removing homologous sequences between and within the sets by CD-HIT-EST at the lowest allowed sequence identity cut-off of 80%. In this dataset each model was trained with TR1+VL1 and tested with TS1. This small training set is used to test the LLM capabilities in a very hard setup for any transfer learning approach.

## Self-supervised RNA-LLM and prediction model

For the comparative analysis, embeddings of each RNA-LLM feed the same deep learning (DL) architecture (Figure 1a-e) for RNA secondary structure prediction. The rationale behind this is that it should not be necessary to optimize the classifier hyperparameters for each LLM, since those have complex architectures and have already been trained with a large amount of data. Thus, according to the transfer learning paradigm, the embeddings should have enough information to solve the downstream task. Moreover, any difference measured in performance will be due to the LLM and not because of the classifier architecture. This is the only trainable part of the experimental setup, which uses the train-test partitions defined for each benchmark dataset.

Sequence one-hot embedding was defined as usual using 4 positions for A, U, G and C (Fig. 1b). Each LLM was used with the pre-trained weights provided, according to instructions in the official repositories. Models were frozen, that is, not re-trained nor fine-tuned. Per-nucleotide embeddings were extracted for each sequence in each benchmark dataset, obtaining a  $d \times L$  tensor, with  $d$  the embedding dimension and  $L$  the sequence length. The embeddings feed the secondary structure prediction network described in Figure 1a. This architecture was designed following the one used in RiNALMo [44], RNA-FM [11], RNA-MSM [78], and ERNIE-RNA [75]. A fully connected layer reduces the input dimension to  $M/2$  (being  $M \ll d$ ), in order to obtain the same dimension for all RNA-LLM. An outer concatenation approach was used to transform the  $M/2 \times L$  projection to a  $M \times L \times L$ . The  $M$  dimension can be interpreted as channels of a  $L \times L$  image. Then, this tensor passes through two 2D ResNet blocks [23] with the following configuration: a first ResNet with convolutions of kernel size 1 and a second one with kernel size 3. Both ResNet blocks include instance Normalization and ReLU activation function. The same DL architecture was trained and tested using each RNA-LLM and dataset. For training, Adam optimizer was used with a learning rate of 0.0001, a batch size of 4 and binary cross-entropy as the loss function. A fixed number of 15 epochs was used in order that all RNA-LLM have equal possibilities for training. The number of epochs and the learning rate were determined in preliminary experiments, ensuring that there was no overfitting nor underfitting of the secondary structure prediction model for any of the RNA-LLM embeddings used as input. Each dataset was used with its own training and testing partitions, except for bpRNA-new, which was only used as a testing partition for the prediction model already trained on bpRNA. All experiments were run on 3 servers, each with 2 NVIDIA RTX A5000 GPU.

For the comparison of RNA-LLM based predictors with baseline methods, the most widely-used pure-thermodynamic structure predictors were included: RNAstructure [46], RNAfold [33] and LinearPartition-V [76]. We have also incorporated hybrid methods, that is, a mix of thermodynamic and machine learning approaches, such as LinearPartition-C [76] and MXFold2 [50]. Finally, we also included the most recent pure DL prediction methods: UFold [18], REDfold [10], and sincFold [7].

## Performance measures

Results are reported with the following performance measures.

**Base pairs metrics:** The focus of performance measures is on the predicted base pairs in comparison to a reference structure [35]. Pairs that are both in the prediction and the reference structure are true positives (TP), while pairs predicted but not in the true structure are false positives (FP). Similarly, a pair in the reference structure that is not predicted is a false negative (FN), and a pair that is neither predicted nor in the true structure is a true negative (TN). A widely used metric is the recall (or sensitivity), defined as the ratio of TP to all the true pairs (TP+FN). It is a measure of how many predicted pairs are true. Instead, the precision is defined as the ratio of TP to all the predicted pairs (TP+FP). This relation between TP and FP is very important in the context of class imbalance, because FP can be a large number in comparison to TP, and this is not reflected in the recall. The  $F_1$  score is the harmonic mean of precision and recall, thus summarizing both measures of performance in a single value. Therefore, in this work the  $F_1$  score is used as the global performance measure for the comparison of the different methods. It is defined as  $F_1 = \frac{2TP}{2TP+FP+FN}$ .

**Structural motifs:** Stems, multiloops, internal loops, bulges, hairpin loops, dangling ends, and external loops were extracted using the bpRNA toolkit [13] on the reference dot-bracket structures. All reference and predicted base-pairs were extracted for positions of each motif type, and average  $F_1$  computed separately.

**Structural similarity:** to complement the  $F_1$  score as an evaluation metric, we have also calculated a structural measure, the Weisfeiler-Lehman graph kernel (WL) metric [48]. The WL metric first assigns to each node (nucleotide) in the graph (secondary structure) a label representing its local structural information. Then, a label propagation step iterates over the nodes and updates their labels based on the labels of their neighboring nodes. Finally, a hash function is computed that aggregates these labels to generate a feature vector. The WL is defined as inner product

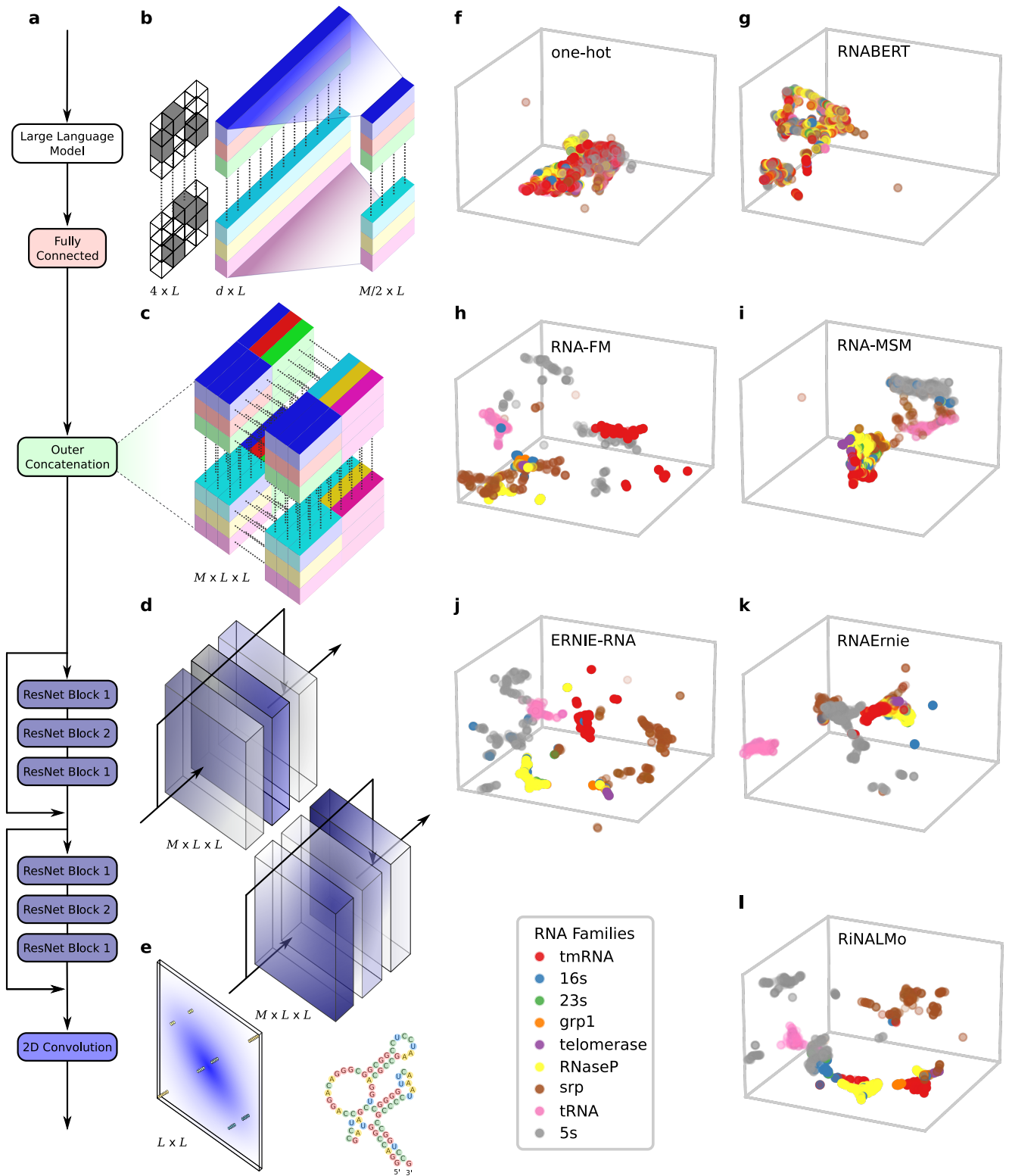


Figure 1 RNA-LLM embeddings and deep neural architecture of the prediction model. **a**, Flow diagram for RNA secondary structure predictions. Each LLM was downloaded from its official repository, frozen and used to get per-nucleotide embeddings for each sequence in the benchmark datasets. The embeddings go through a fully connected layer, outer concatenation, two 2D ResNet blocks and a final 2D convolution. This flow is explained in detail in aligned panels b-e. **b**, One-hot encoding, of size  $4 \times L$ , and LLM representation with size  $d \times L$ , where  $d$  is the embedding dimension and  $L$  is the padded sequence length. A fully connected layer reduces the input dimension to  $M/2$ . **c**, The  $M/2 \times L$  projection is transformed to a  $M \times L \times L$  tensor using outer concatenation. The position  $(i, j)$  contains the concatenated representation of nucleotides  $i$  and  $j$ . **d**, Then, there are two 2D ResNet blocks with 2D Convolution, Instance Normalization and ReLU. ResNet Blocks 1 has kernel size 1 and ResNet Blocks 2 has kernel size 3. **e**, A final convolution yields the output scores as a  $L \times L$  connection matrix. **f-l**, RNA-LLM embeddings projected with UMAP for dimensionality reduction. The RNA families of the ArchiveII dataset are highlighted with different colors. Sequences within the same RNA family are expected to be close in the dimensionally reduced space.

$WL(G_1, G_2) = \Phi(G_1) \cdot \Phi(G_2)$ , where  $\Phi(G_i)$  represents the feature vector of graph  $G_i$  obtained by aggregating the labels through the hash function.

## Results

### LLM separate structural families even when they were not pre-trained with family information

A useful RNA embedding for the RNA secondary structure prediction task is expected to well-represent not only sequence properties, but also structural aspects. Therefore, RNA embeddings encoding similar features should share a common region in the multidimensional embedding space. To have a preliminary insight into this topic, a qualitative comparison of LLM embeddings of the ArchiveII dataset was performed by nonlinearly reducing them to three dimensions using the uniform manifold approximation and projection (UMAP) [37]. After that, each RNA sequence was depicted with a different color according to its corresponding RNA family (Fig. 1f-1).

The one-hot encoding (Fig. 1f) was used as reference. In this case, as for RNABERT (Fig. 1g) representations, there is a large overlap and mixing of sequences that belong to different RNA families; that is, in the same close region there are sequences that are very different in length, structure, and function. Instead, in the case of RNA-FM (Fig. 1h), ERNIE-RNA (Fig. 1j) and RiNALMo (Fig. 1l) each RNA family is mostly separated from the others. The 5s family (gray), which is the largest family, is distributed in several regions of the projected space. In the case of RNA-FM, the 5s, tmRNA (red) and tRNA (pink) families are well-separated among them. Overall, it can be stated that for RiNALMo and ERNIE-RNA, most RNA sequences and families are well-separated in the 3D projected space. In the case of RNA-MSM (Fig. 1i), there are two large and separated clusters but with a mix of families within. One large cluster has tmRNA, RNaseP (yellow), srp (brown), 23s (green), and telomerase (violet); while the other cluster has 5s, srp and tRNA. RNAErnie has a mix of very well-separated and cohesive groups of sequences belonging to the families tRNA, srp and 5s; but there is also a large overlap among sequences of the other families. The telomerase family, the longest one, can hardly be distinguished in any case, being cohesively and separately represented only in the case of RiNALMo and ERNIE-RNA.

### Performance on homology-challenging datasets

Figure 2 shows the comparative results among the RNA-LLM here reviewed in terms of  $F_1$  violin plots. In each plot the results are presented in order, from best (left) to worst (right) median  $F_1$ . The best thermodynamic and DL-based predictors were used as baselines in the plots (details in Supplementary Table 1).

Figure 2a shows the results for 5-fold random partitions on the ArchiveII dataset. It can be seen that most predictors achieve a median performance above  $F_1 = 0.60$ , except only for the one based on one-hot encoding ( $F_1 = 0.57$ ). The top-3 RNA-LLM achieve a very high performance ( $F_1 > 0.90$ ). Those are ERNIE-RNA and RiNALMo, both with  $F_1 = 0.95$ , and RNA-FM with  $F_1 = 0.91$ . RNAErnie and RNA-MSM achieve an intermediate performance,  $F_1 = 0.76$  and  $F_1 = 0.74$ , respectively. Finally, RNABERT is the RNA-LLM with the lowest average performance ( $F_1 = 0.62$ ). For this random  $k$ -folding, all RNA-LLM achieve higher performance than the classical prediction method ( $F_1 = 0.61$ ). Remarkably here, the DL-based method achieves the highest median performance ( $F_1 = 0.97$ ). This result shows that the neural architecture used in the classifier has the capability of obtaining high performance in predictions. However, it is well-known that the sequence homology between train and test at random partitions favors methods based on deep learning; thus performance tends to be overly optimistic.

For a deeper analysis, we have extended the experiments on standard datasets having controlled levels of homology between training and testing partitions. Figure 2b shows the test  $F_1$  for bpRNA dataset, with a partition at 80% sequence-identity cutoff between training (TR0+VL0) and testing (TS0).

The results show that now, in a harder testing setup, most methods lowered performance in comparison to random partitions. Here, again, ERNIE-RNA and RiNALMo have both the best median scores in the test set, but in this case with a large drop in performance:  $F_1 = 0.68$  and  $F_1 = 0.64$ , respectively. These two RNA-LLM are the only ones that achieve better performance than the classical prediction method ( $F_1 = 0.53$ ) and very close performance to the DL-based method ( $F_1 = 0.68$ ). With median performance below it, RNA-FM has  $F_1 = 0.52$ , RNA-MSM has  $F_1 = 0.42$ , and RNAErnie has  $F_1 = 0.41$ . Both one-hot and RNABERT reached similar and very poor results,  $F_1 = 0.35$  and  $F_1 = 0.33$ , respectively.

Figure 2c shows the results of testing already trained models with the bpRNA-new dataset, which was designed to evaluate the prediction on new RNA families, never seen during training. The performance of all methods has been noticeably reduced, being the medians of almost all RNA-LLM below the classical folding method ( $F_1 = 0.67$ ). The only RNA-LLM with the same performance as the classical one is ERNIE-RNA. In all the other cases, the median  $F_1$  is below 0.45. RiNALMo achieved the same median performance as the DL-based baseline ( $F_1 = 0.44$ ). Additionally, note that the one-hot encoding moved up one more position in the ranking, slightly outperforming RNAErnie in this test set. This large dataset was used to analyze the prediction scores per structural motif, as seen in Figure 2e. It can be seen that most models behave similarly for each motif type, with ERNIE-RNA showing a higher performance in stem base-pair predictions. Overall, ERNIE-RNA, RiNALMo and RNA-MSM achieved the best scores for each motif.

Results on a more challenging dataset, closer to a real-world application, are shown in Figure 2d, where every RNA-LLM was tested in a set of 62 RNA sequences whose secondary structures were inferred from high-resolution RNA

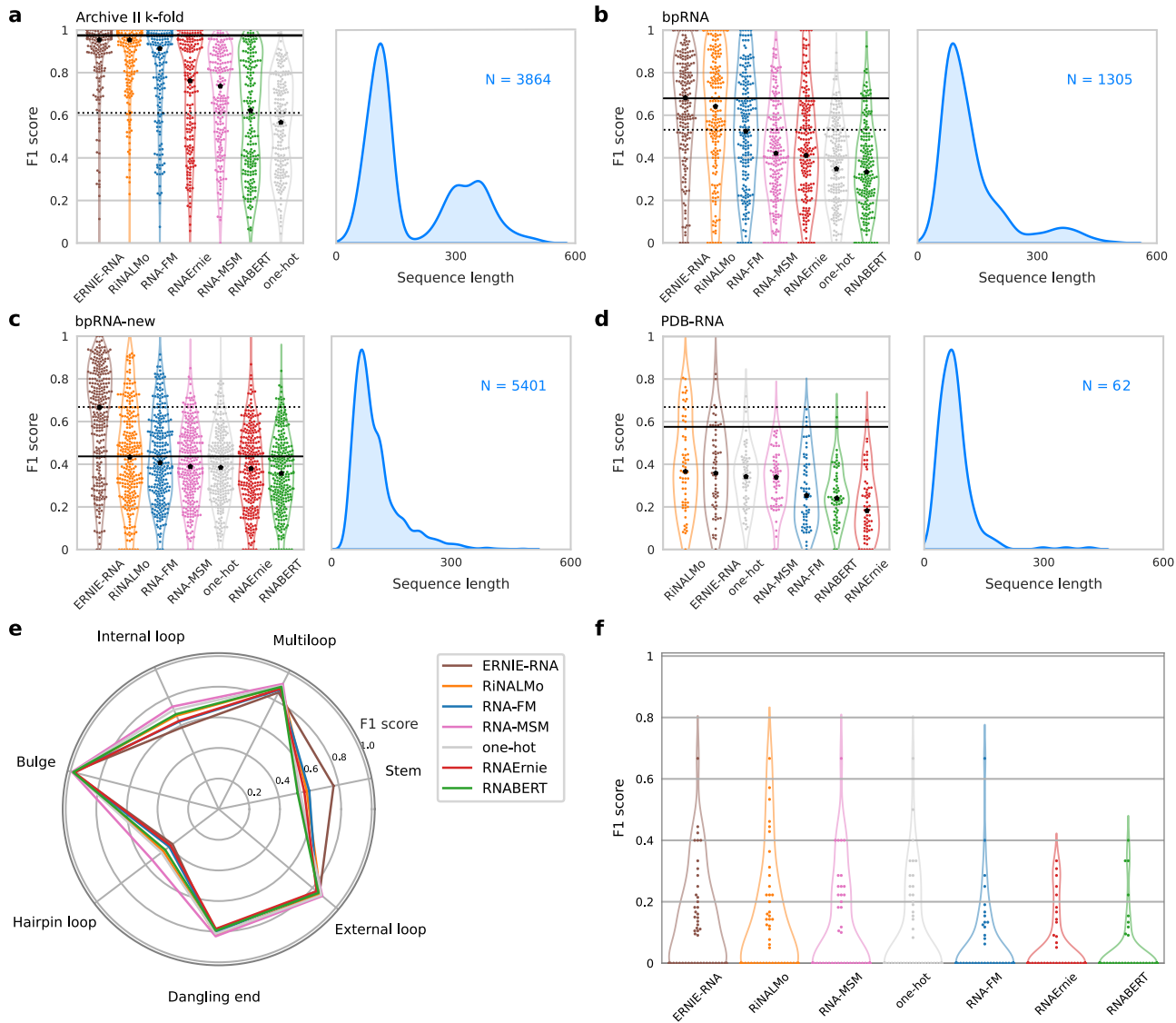


Figure 2 Comparative results among RNA-LLM on the RNA secondary structure prediction task for different benchmark datasets of increasing complexity. Each method has a different color. The thermodynamic prediction method (LinearPartition-V, dashed black) and the DL-based prediction method (sincFold, solid black line) are added as baselines. Next to RNA-LLM performances, sequence length distribution for each dataset is shown in blue. **a**, ArchiveII 5-fold random cross-validation. A Wilcoxon test for paired samples with Bonferroni correction indicates that all differences are statistically significant ( $P < 0.0001$ ,  $N = 3,864$ ). **b**, bpRNA train-test partitions with controlled homology. All differences are statistically significant ( $P < 0.0001$ ,  $N = 1,305$ ) except for one-hot and RNABERT. **c**, bpRNA-new dataset, for RNA families not seen during training. All differences are statistically significant ( $P < 0.0001$ , except for RNAErnie versus RNA-MSM and one-hot with  $P < 0.05$ ,  $N = 5,401$ ). **d**, PDB-RNA dataset, with RNA sequences extracted from PDB. Most differences are not statistically significant among RNA-LLM, except for RiNALMo and ERNIE-RNA with respect to RNA-FM, RNABERT and RNAErnie. Details of statistical analysis in Supplementary Fig. S1a-d. **e**, Average  $F_1$  per motif type on bpRNA-new. **f**, Performance accounting only non-canonical interactions on PDB-RNA.

X-ray 3D structures from the PDB dataset. Results clearly show a hard fall in results for all the RNA-LLM, with median performances below  $F_1 = 0.40$ , lower than the classical folding method ( $F_1 = 0.67$ ) and the DL-based method ( $F_1 = 0.58$ ). Notably in this dataset, the one-hot encoding is within the top-3 methods, outperforming RNA-FM, RNAErnie and RNABERT; with almost the same performance that RNA-MSM, ERNIE-RNA and RiNALMo. It can be said that, for this prediction challenge, no RNA-LLM provides significant improvements of transfer learning over a one-hot encoding. This dataset also contains non-canonical interactions, although most of the methods fail to reach a median  $F_1$  score higher than 0.2 (Fig. 2f), with a slightly better performance for ERNIE-RNA and RiNALMo.

Additionally to the  $F_1$  score, we have also calculated for all the datasets analyzed the WL metric, which was proposed to capture structural information between predictions and the corresponding references. Supplementary Table 1 shows that the performances have the same trend to those results reported and analyzed with  $F_1$ .

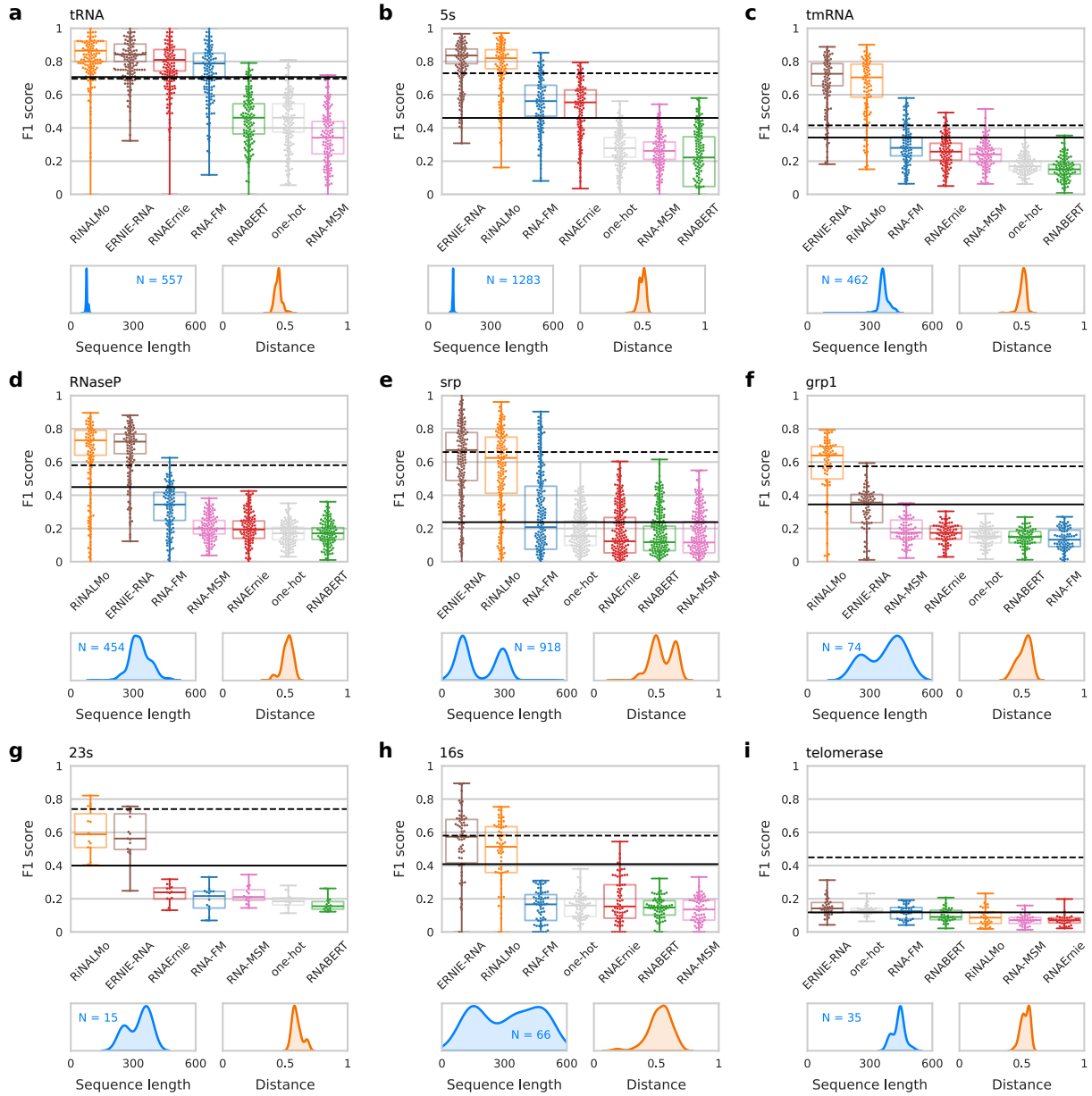


Figure 3 Inter-family structure prediction based on RNA LLM. Performance evaluated on the 9 RNA families of the ArchiveII dataset. Each boxplot represents the  $F_1$  performance of all methods for a given family in the test set. The thermodynamic prediction method (LinearPartition-V, dashed black) and the DL-based method (sincFold, solid black line) are added as baselines in all plots. Below RNA-LLM performances, sequence length distribution for each dataset is shown in blue and distribution of minimum test-train structural distance [46] is shown in orange. **a**, tRNA family. A Wilcoxon test for paired samples with Bonferroni correction indicates that all differences are statistically significant ( $P < 0.0001$ ,  $N = 557$ ), except in the case of RiNALMo with ERNIE-RNA, and RNABERT with one-hot. **b**, 5s family. All differences are statistically significant ( $P < 0.0001$ ,  $N = 1283$ ). **c**, tmRNA family. All differences are statistically significant ( $P < 0.0001$ ,  $N = 462$ ). **d**, RNaseP family. Only ERNIE-RNA with RiNALMo, RNA-MSM with RNAErnie, and one-hot with RNABERT are not statistically significant. **e**, srp family. Differences for the top 4 methods are statistically significant ( $P < 0.0001$ ,  $N = 918$ ). **f**, grp1 family. Differences for the top 2 methods are statistically significant ( $P < 0.0001$ ,  $N = 74$ ). **g**, 23s family. Top 2 methods are significantly better than the rest of all the methods ( $P < 0.01$ ,  $N = 15$ ). **h**, 16s family. RiNALMo and ERNIE-RNA are statistically different and are also statistically different from the rest of the methods ( $P < 0.0001$ ,  $N = 66$ ). **i**, telomerase family. ERNIE-RNA and one-hot are statistically different from RNABERT, RiNALMo, RNA-MSM and RNAErnie. Details of statistical analysis in Supplementary Fig. S2.

## Cross-family benchmarks

For assessing inter-family performance, a family-fold cross validation in the ArchiveII dataset was performed. That is, one family was left out for testing per cross-validation fold, and the rest of the families were used for training. This eliminates most of the homology to the training set, providing a hard measure of performance and, thus, allowing estimating future

performance on novel RNAs that do not belong to any known family. These results are shown in Figure 3, along with the distributions of sequence lengths and minimum structural distances [46] between each test sequence and all the sequences in its corresponding training fold. The best thermodynamic and DL-based predictors are shown as reference for comparison in the plots (detailed results in Supplementary Table 2).

In the case of the tRNA family (Fig. 3a), the one with the shortest sequence length as shown in the panel below, most methods achieve performance above  $F_1 = 0.40$ . RNABERT and one-hot achieved both the same performance here, close to  $F_1 = 0.46$ . The four best methods for this family are RiNALMo ( $F_1 = 0.86$ ), ERNIE-RNA ( $F_1 = 0.84$ ), RNAErnie ( $F_1 = 0.81$ ) and RNA-FM ( $F_1 = 0.79$ ). In this case, which can be considered the easiest one for a cross-family validation due to the small length of sequences and test/train structural distance below 0.5, four of the RNA-LLM outperform both the classical method, which achieved  $F_1 = 0.70$ , and the DL-based model, which achieved  $F_1 = 0.71$ . For the 5s family (Fig. 3b), the results for all RNA-LLM are very similar to the previous family, again due to the length of the sequences (the second mean shortest family) and low structural distance between this family and all the remaining families in the training set. In this case, one-hot representation, RNABERT and RNA-MSM are below  $F_1 = 0.26$ , while RNAErnie and RNA-FM achieve performances around  $F_1 = 0.55$ , and again ERNIE-RNA and RiNALMo achieved both the best results, with  $F_1 = 0.84$  and  $F_1 = 0.82$ , respectively, above the classical method ( $F_1 = 0.73$ ). The DL-based model achieved  $F_1 = 0.46$  here, below RNAErnie and RNA-FM. For the tmRNA (Fig. 3c) and RNaseP (Fig. 3d) families, the conclusions are very similar as before. Although ERNIE-RNA and RiNALMo have performance 10% lower than with the previous families, in these cases achieved even higher performance than both the classical and the DL-based method. In the case of the tmRNA family (Fig. 3c), the classical method has  $F_1 = 0.42$  and the DL-based has  $F_1 = 0.34$ , while ERNIE-RNA and RiNALMo have almost twice the performance with  $F_1 = 0.73$ . In the case of the RNaseP (Fig. 3d) family, those two RNA-LLM methods are more than 10% better than the classical and the DL-based method. Here, it is important to note that these two families are very similar to each other in average sequence length, around 300 nt, but 3 times longer than tRNA and 5s families.

In the case of the srp family (Fig. 3e), there is an important change in the length distribution, which becomes bimodal, and in the structural distances distribution, which clearly exceeds the 0.5 mark. Here, the classical method, ERNIE-RNA and RiNALMo achieve extremely close results while all other RNA-LLM and the DL-based method are far below them. ERNIE-RNA has median  $F_1 = 0.67$  while the classical method achieved  $F_1 = 0.66$ . Notably, in the case of the grp1 family (Fig. 3f), which has larger average length size than srp, RiNALMo is the only LLM that clearly outperforms all methods, even the classical one ( $F_1 = 0.64$  versus  $F_1 = 0.57$ ). In the second position, ERNIE-RNA achieves the same performance as the DL-based method. In the case of the 23s and 16s families (Figs. 3g and 3h, respectively), it can be seen that the one-hot representation, RNABERT, RNA-FM, RNA-MSM and RNAErnie embeddings are all below  $F_1 = 0.25$ , a very low performance. However, ERNIE-RNA and RiNALMo achieve almost twice that performance with median values near to  $F_1 = 0.60$ , and the classical method achieves better results ( $F_1 = 0.74$  for 23s and  $F_1 = 0.58$  for 16s). The DL-based method presents intermediate results:  $F_1 = 0.40$  for 23s and  $F_1 = 0.41$  for 16s.

Notably, this last family has a wide variety of sequence lengths and structural distances. Finally when the telomerase family (Fig. 3i) is used in the test set, all RNA-LLM and the DL-based method achieve extremely poor results below  $F_1 = 0.15$ . This family has the longest sequences. Here the classical method has a large advantage over all RNA-LLM ( $F_1 = 0.45$ ), although it is low compared to the other families.

For these dataset partitions we have also calculated the WL metric, showing performance trends similar to those analyzed for  $F_1$  score (see details in Supplementary Table 2).

## Discussion

We benchmarked 6 RNA-LLM for their ability to predict RNA secondary structure based only on the sequence, in 4 datasets of increasing complexity. First we performed a visual comparison of the LLM embeddings with a UMAP projection, analyzing the distribution and separation of the RNA families. We found that RiNALMo and ERNIE-RNA were the models that could better represent and separate the RNA families in the projection without almost overlap. Notably, as Table 1 shows, those RNA-LLM are the biggest ones, pre-trained with the largest and most varied datasets.

We tested each RNA-LLM implementation with exactly the same experimental setup and deep neural network architecture for RNA secondary structure prediction in several benchmark datasets, increasing the difficulty from simple random partitions to very low homology between training and testing partitions. Overall, RiNALMo and ERNIE-RNA maintained an acceptable level of generalization capability even in the hardest test, providing equivalent performance to the classical folding method. Remarkably, in that hardest scenario the trivial one-hot representation achieved a performance similar to the best performing RNA-LLM. Thanks to the transfer learning paradigm, one would have expected that LLM would help to generalize even with a small training set and prediction model, because all the relevant information was learnt in the embeddings. That was not the case and it was probably an indication that there is still important information that cannot be fully captured even by the LLM pre-training. The results achieved might be explained by the fact that the structures of sequences in the testing sets were really very different from those seen during pre-training, or they were a small minority, thus the generalization capability of the prediction model could not be really benefited from using a LLM representation.

Precisely regarding the information that may have been incorporated in the pre-training of the RNA-LLMs, it is interesting to compare them with methods that use homology information for predicting RNA secondary structures [5,

21, 73, 51, 22, 69]. In the case of the dataset closest to a real-world application, PDB-RNA (Figure 2d), Singh et al. [55] reviewed the most relevant methods that use homology information with the following performance: CentroidAlifold [21]  $F_1 = 0.69$ , TurboFold II [65]  $F_1 = 0.64$ , RNAalifold [5]  $F_1 = 0.66$  and CentroidFold [49]  $F_1 = 0.60$ . These performances are extremely close to the baseline performance of the pure thermodynamic method ( $F_1 = 0.67$ , Figure 2d), and those are actually the highest performance values for this dataset. Instead, here all RNA-LLM show very poor results, with median performances below  $F_1 = 0.40$ . Thus, there is still a large performance gap between RNA LLM based and classical methods, independently of explicit homology incorporation. Remarkably, the best DL-based method, without using any homology nor alignment data, has achieved an intermediate performance within the gap mentioned ( $F_1 = 0.58$ ), even very close to some of the homology-based methods. It is also interesting to compare RNA-LLM trained only with RNA sequences with approaches that incorporate other information in pre-training. Multimodal LLM are interesting since they propose new ways of gaining insights in related data distributions. For example, Evo [41] was trained with DNA, considering coding and non-coding sequences. However, since this is fundamentally a generative model trained for sequence design with large contexts, the internal representations obtained for RNA sequences from our datasets were not successful to predict secondary structures. Other methods use abundant DNA sequences in a BERT-like architecture such as DNABERT2 [79]. In this case, the performance of the DNABERT2 model in the datasets here evaluated was just slightly better than RNABERT. From these results, it can be concluded that LLM are still unable to correctly represent the additional information incorporated in the pre-training stage, or if they were able to capture it, it is not trivial to extract this extra information with the models in the downstream tasks.

For the most difficult secondary structure prediction task, we removed from training all the sequences of one specific testing family. In this setup, most of the RNA-LLM achieved a high performance for the two shortest families. However, as the average length of the sequence to be predicted increased, the performance of most RNA-LLM lowered below  $F_1 = 0.50$ . Overall, in 4 out of 9 cases RiNALMo and ERNIE-RNA outperformed the classical method. In two cases no differences were observed, and in the last three families the classical method was the best. In the case of the telomerase RNA family, the most different from the other ones, with very few samples in all datasets and the largest average sequence length, the results were all poor, up to three times below the classical method. In any case, in this RNA family the classical method also obtained a performance without practical usefulness, barely reaching  $F_1 = 0.50$ . Remarkably, in this hard prediction task, RiNALMo and ERNIE-RNA always outperformed the DL-based prediction method.

Our study showed that RNA-LLM in combination with a deep neural network for prediction were surprisingly capable of outperforming a classical method in half of the RNA families, even though cross-family prediction was a task historically dominated by thermodynamic methods. Although in this study we have not delved into the analysis of classical methods, because those are outside the scope of the RNA-LLM comparison, it is important to note that their historical superiority is due to a limited understanding of the concept of data-driven learning. This is intuitively associated only to machine learning methods, but all thermodynamics-based methods also have data-driven learning. For machine learning-based methods, humans build a software with rules to be trained automatically from domain examples, thus excluding some of those examples for testing is very simple. Conversely, for classical methods humans learn themselves from data samples, and then build a software with those learned rules. That is: they observe many sequences and structures for years, test and improve their models based on those observations, and even incorporate measurements of real structures as parameters of their models [36]. In these cases, it is much more difficult to simply exclude training samples from testing sets. This is why a new methodology is required to make a fairer comparison with thermodynamic methods.

We found that those RNA-LLM trained in the self-supervised stage with the largest and most varied number of sequences, and with the largest number of trainable parameters (ERNIE-RNA and RiNALMo), were also those that better represented the different RNA families in the projected UMAP space and those that accordingly achieved higher performance overall, very consistently and in all cases. At the same time, our experimental design clearly revealed the most important challenges that remain unsolved in RNA secondary structure prediction yet. We generated the first systematic benchmarking for this prediction task with LLM. Our experimental methodology, the curated datasets and the full source code are a key tool for analysts to navigate the space of available RNA-LLM methods, and constitutes a reference base for developers towards building more efficient prediction methods. We are confident that the criteria and analysis processes defined here can become a benchmark for future systematic investigations of RNA-LLM performance.

## References

- [1] Manato Akiyama and Yasubumi Sakakibara. Informative RNA base embedding for RNA structural alignment and clustering by deep representation learning. *NAR Genomics and Bioinformatics*, 4(1), 2022.
- [2] Ethan C. Alley, Grigory Khimulya, Surojit Biswas, Mohammed AlQuraishi, and George M. Church. Unified rational protein engineering with sequence-based deep representation learning. *Nature Methods*, 16(12):1315–1322, 2019.
- [3] Noorul Amin, Annette McGrath, and Yi-Ping Phoebe Chen. Evaluation of deep learning in non-coding rna classification. *Nature Machine Intelligence*, 1(5):246–256, 2019.
- [4] Ehsaneddin Asgari and Mohammad R. K. Mofrad. Continuous distributed representation of biological sequences for deep proteomics and genomics. *PLOS ONE*, 10(11):1–15, 2015.

- [5] Stephan H Bernhart, Ivo L Hofacker, Sebastian Will, Andreas R Gruber, and Peter F Stadler. Rnaalifold: improved consensus structure prediction for rna alignments. *BMC Bioinformatics*, 9(1), November 2008.
- [6] Edouard Bonnet, Pawel Rzazewski, and Florian Sikora. Designing RNA secondary structures is hard. *Journal of Computational Biology*, 27(3):302–316, 2020.
- [7] Leandro A Bugnon, Leandro Di Persia, Matias Gerard, Jonathan Raad, Santiago Prochetto, Emilio Fenoy, Uciel Chorostecki, Federico Ariel, Georgina Stegmayer, and Diego H Milone. sincFold: end-to-end learning of short- and long-range interactions in rna secondary structure. *Briefings in Bioinformatics*, 25(4):bbae271, May 2024.
- [8] Xinang Cao, Yueying Zhang, Yiliang Ding, and Yue Wan. Identification of RNA structures and their roles in RNA functions. *Nature Reviews Molecular Cell Biology*, 25:784–801, 2024.
- [9] Thomas R. Cech and Joan A. Steitz. The noncoding RNA revolution—trashing old rules to forge new ones. *Cell*, 157(1):77–94, 2014.
- [10] Chun-Chi Chen and Yi-Ming Chan. REDfold: accurate RNA secondary structure prediction using residual encoder-decoder network. *BMC Bioinformatics*, 24(1), 2023.
- [11] Jiayang Chen and et al. Interpretable RNA foundation model from unannotated data for highly accurate RNA structure and function predictions. *arXiv*, 1(1):1–10, 2022.
- [12] Ke Chen, Thomas Litfin, Jaswinder Singh, Jian Zhan, and Yaoqi Zhou. Mars and rnaCmap3: The master database of all possible RNA sequences integrated with RNACmap for RNA homology search. *Genomics, Proteomics and Bioinformatics*, 22(1), 2024.
- [13] Padideh Danaee, Mason Rouches, Michelle Wiley, Dezhong Deng, Liang Huang, and David Hendrix. bpRNA: large-scale automated annotation and analysis of RNA secondary structure. *Nucleic Acids Research*, 46(11):5381–5394, May 2018.
- [14] Tri Dao. Flashattention-2: Faster attention with better parallelism and work partitioning. *arXiv*, 1(1):1–10, 2023.
- [15] Jacob Devlin, Ming-Wei Chang, Kenton Lee, and Kristina Toutanova. Bert: Pre-training of deep bidirectional transformers for language understanding. *North American Chapter of the Association for Computational Linguistics*, 1:4171–4186, 2019.
- [16] Jacob Devlin, Ming-Wei Chang, Kenton Lee, and Kristina Toutanova. Bert: Pre-training of deep bidirectional transformers for language understanding. In *North American Chapter of the Association for Computational Linguistics*, 2019.
- [17] Ahmed Elnaggar and et al. Prototrans: Towards cracking the language of life’s code through self-supervised deep learning and high performance computing. *IEEE Transactions on Pattern Analysis and Machine Intelligence*, 1(1):1–10, 2021.
- [18] Laiyi Fu, Yingxin Cao, Jie Wu, Qinke Peng, Qing Nie, and Xiaohui Xie. Ufold: Fast and accurate RNA secondary structure prediction with deep learning. *Nucleic Acids Research*, 50(3):e14, 2022.
- [19] Limin Fu, Beifang Niu, Zhengwei Zhu, Sitao Wu, and Weizhong Li. Cd-hit: accelerated for clustering the next-generation sequencing data. *Bioinformatics*, 28(23):3150–3152, 2012.
- [20] Laura R. Ganser, Megan L. Kelly, Daniel Herschlag, and Hashim M. Al-Hashimi. The roles of structural dynamics in the cellular functions of rnas. *Nature Reviews Molecular Cell Biology*, 20(8):474–489, 2019.
- [21] Michiaki Hamada, Kengo Sato, and Kiyoshi Asai. Improving the accuracy of predicting secondary structure for aligned rna sequences. *Nucleic Acids Research*, 39(2):393–402, September 2010.
- [22] Michiaki Hamada, Kengo Sato, Hisanori Kiryu, Toutai Mituyama, and Kiyoshi Asai. Predictions of rna secondary structure by combining homologous sequence information. *Bioinformatics*, 25(12):i330–i338, May 2009.
- [23] Kaiming He, Xiangyu Zhang, Shaoqing Ren, and Jian Sun. Deep residual learning for image recognition. *Proceedings of the IEEE Conference on Computer Vision and Pattern Recognition (CVPR)*, 1:770–778, 2016.
- [24] Michael Heinzinger, Ahmed Elnaggar, Yu Wang, Christian Dallago, Dmitrii Nechaev, Florian Matthes, and Burkhard Rost. Modeling aspects of the language of life through transfer-learning protein sequences. *BMC Bioinformatics*, 20(1):723, 2019.
- [25] Hyeonseo Hwang, Hyeonseong Jeon, Nagyeong Yeo, and Daehyun Baek. Big data and deep learning for RNA biology. *Experimental and Molecular Medicine*, 56:1293–1321, 2024.
- [26] Thomas R. Cech John F. Atkins, Raymond F. Gesteland. *RNA worlds: from life’s origins to diversity in gene regulation*. Cold Spring Harbor, New York, 2011.

- [27] John Jumper and et al. Highly accurate protein structure prediction with alphafold. *Nature*, 596(7873):583–589, 2021.
- [28] Ioanna Kalvari and et al. Rfam 13.0: shifting to a genome-centric resource for non-coding RNA families. *Nucleic Acids Research*, 46(D1):D335–D342, 2017.
- [29] Ioanna Kalvari and et al. Rfam 14: expanded coverage of metagenomic, viral and microRNA families. *Nucleic Acids Research*, 49(D1):D192–D200, 2021.
- [30] Neocles B Leontis, Aurelie Lescoate, and Eric Westhof. The building blocks and motifs of RNA architecture. *Current Opinion in Structural Biology*, 16(3):279–287, 2006.
- [31] Francesca-Zhoufan Li, Ava P. Amini, Yisong Yue, Kevin K. Yang, and Alex X. Lu. Feature reuse and scaling: Understanding transfer learning with protein language models. *arXiv*, pages 1–10, 2024.
- [32] Jiajia Liu, Mengyuan Yang, Yankai Yu, Haixia Xu, Kang Li, and Xiaobo Zhou. Large language models in bioinformatics: applications and perspectives. *arXiv*, pages 1–12, 2024.
- [33] Ronny Lorenz, Stephan H Bernhart, Christian Höner zu Siederdisen, Hakim Tafer, Christoph Flamm, Peter F Stadler, and Ivo L Hofacker. ViennaRNA package 2.0. *Algorithms for Molecular Biology*, 6(1):1–10, November 2011.
- [34] Fergal J Martin, M Ridwan Amode, Alisha Aneja, Olanrewaju Austine-Orimoloye, and et al. Ensembl 2023. *Nucleic Acids Research*, 51(D1):D933–D941, 2022.
- [35] David H. Mathews. How to benchmark RNA secondary structure prediction accuracy. *Methods*, 162-163:60–67, June 2019.
- [36] David H. Mathews, Matthew D. Disney, Jessica L. Childs, Susan J. Schroeder, Michael Zuker, and Douglas H. Turner. Incorporating chemical modification constraints into a dynamic programming algorithm for prediction of RNA secondary structure. *Proceedings of the National Academy of Sciences*, 101(19):7287–7292, May 2004.
- [37] Leland McInnes, John Healy, Nathaniel Saul, and Lukas Großberger. Umap: Uniform manifold approximation and projection. *Journal of Open Source Software*, 3(29):861, 2018.
- [38] Seonwoo Min, Byunghan Lee, and Sungroh Yoon. Deep learning in bioinformatics. *Briefings in Bioinformatics*, 18(5):851–869, 2017.
- [39] Seonwoo Min, Seunghyun Park, Siwon Kim, Hyun-Soo Choi, Byunghan Lee, and Sungroh Yoon. Pre-training of deep bidirectional protein sequence representations with structural information. *IEEE Access*, 9(1):123912–123926, 2021.
- [40] Stefanie A. Mortimer, Mary Anne Kidwell, and Jennifer A. Doudna. Insights into RNA structure and function from genome-wide studies. *Nature Reviews Genetics*, 15(7):469–479, 2014.
- [41] Eric Nguyen, Michael Poli, Matthew G. Durrant, Brian Kang, Dhruva Katrekar, David B. Li, Liam J. Bartie, Armin W. Thomas, Samuel H. King, Garyk Brixi, Jeremy Sullivan, Madelena Y. Ng, Ashley Lewis, Aaron Lou, Stefano Ermon, Stephen A. Baccus, Tina Hernandez-Boussard, Christopher Ré, Patrick D. Hsu, and Brian L. Hie. Sequence modeling and design from molecular to genome scale with evo. *Science*, 386(6723):eado9336, 2024.
- [42] Norbert Pardi, Michael J. Hogan, Frederick W. Porter, and Drew Weissman. mRNA vaccines — a new era in vaccinology. *Nature Reviews Drug Discovery*, 17(4):261–279, 2018.
- [43] Di Peng, Liubin Zheng, Dan Liu, Cheng Han, Xin Wang, Yan Yang, Li Song, Miaoying Zhao, Yanfeng Wei, Jiayi Li, Xiaoxue Ye, Yuxiang Wei, Zihao Feng, Xinhe Huang, Miaomiao Chen, Yujie Gou, Yu Xue, and Luoying Zhang. Large-language models facilitate discovery of the molecular signatures regulating sleep and activity. *Nature Communications*, 15(1):3685–3690, 2024.
- [44] Rafael Josip Penić, Tin Vlašić, Roland G. Huber, Yue Wan, and Mile Šikić. Rinalmo: General-purpose RNA language models can generalize well on structure prediction tasks. *arXiv*, 1(1):1–10, 2024.
- [45] Roshan Rao and et al. Evaluating protein transfer learning with TAPE. *CoRR*, abs/1906.08230, 2019.
- [46] Jessica S Reuter and David H Mathews. RNAstructure: software for RNA secondary structure prediction and analysis. *BMC Bioinformatics*, 11(1):1–10, March 2010.
- [47] Alexander Rives and et al. Biological structure and function emerge from scaling unsupervised learning to 250 million protein sequences. *Proceedings of the National Academy of Sciences*, 118(15):e2016239118, 2021.
- [48] Frederic Runge, Jörg K. H. Franke, Daniel Fertmann, and et al. Rethinking performance measures of rna secondary structure problems. *NeuIPs 2023 - Machine Learning in Structural Biology Workshop*, 1:1–12, 2023.

- [49] K. Sato, M. Hamada, K. Asai, and T. Mituyama. Centroidfold: a web server for rna secondary structure prediction. *Nucleic Acids Research*, 37(Web Server):W277–W280, May 2009.
- [50] Kengo Sato, Manato Akiyama, and Yasubumi Sakakibara. RNA secondary structure prediction using deep learning with thermodynamic integration. *Nature Communications*, 12(1):1–10, February 2021.
- [51] Kengo Sato, Yuki Kato, Tatsuya Akutsu, Kiyoshi Asai, and Yasubumi Sakakibara. Dafs: simultaneous aligning and folding of rna sequences via dual decomposition. *Bioinformatics*, 28(24):3218–3224, October 2012.
- [52] Eric W Sayers and et al. Database resources of the national center for biotechnology information in 2023. *Nucleic Acids Research*, 51(D1):D29–D38, 2022.
- [53] Noam Shazeer. Glu variants improve transformer. *arXiv*, 1(1):1–10, 2020.
- [54] Jaswinder Singh, Jack Hanson, Kuldip Paliwal, and Yaoqi Zhou. RNA secondary structure prediction using an ensemble of two-dimensional deep neural networks and transfer learning. *Nature Communications*, 10(1), November 2019.
- [55] Jaswinder Singh, Kuldip Paliwal, Tongchuan Zhang, Jaspreet Singh, Thomas Litfin, and Yaoqi Zhou. Improved RNA secondary structure and tertiary base-pairing prediction using evolutionary profile, mutational coupling and two-dimensional transfer learning. *Bioinformatics*, 37(17):2589–2600, March 2021.
- [56] Michael F. Sloma and David H. Mathews. Exact calculation of loop formation probability identifies folding motifs in RNA secondary structures. *RNA*, 22(12):1808–1818, October 2016.
- [57] Martin Steinegger and Johannes Söding. Mmseqs2 enables sensitive protein sequence searching for the analysis of massive data sets. *Nature Biotechnology*, 35(11):1026–1028, 2017.
- [58] Eric J. Strobel, Angela M Yu, and Julius B. Lucks. High-throughput determination of RNA structures. *Nature Reviews Genetics*, 19(10):615–634, 2018.
- [59] Jianlin Su, Murtadha Ahmed, Yu Lu, Shengfeng Pan, Wen Bo, and Yunfeng Liu. Roformer: Enhanced transformer with rotary position embedding. *Neurocomputing*, 568:127063, 2024.
- [60] Yu Sun, Shuohuan Wang, Yukun Li, Shikun Feng, Xuyi Chen, Han Zhang, Xin Tian, Danxiang Zhu, Hao Tian, and Hua Wu. Ernie: Enhanced representation through knowledge integration. *ArXiv*, abs/1904.09223, 2019.
- [61] Yu Sun, Shuohuan Wang, Yukun Li, Shikun Feng, Hao Tian, Hua Wu, and Haifeng Wang. Ernie 2.0: A continual pre-training framework for language understanding. *Proceedings of the AAAI Conference on Artificial Intelligence*, 34(05):8968–8975, 2020.
- [62] Blake A Sweeney and et al. Rnacentral 2021: secondary structure integration, improved sequence search and new member databases. *Nucleic Acids Research*, 49(D1):D212–D220, 2020.
- [63] Artur Szalata, Karin Hrovatin, Sören Becker, Alejandro Tejada-Lapuerta, Haotian Cui, Bo Wang, and Fabian J. Theis. Transformers in single-cell omics: a review and new perspectives. *Nature Methods*, 21(8):1430–1443, 2024.
- [64] Marcell Szikszai, Michael Wise, Amitava Datta, Max Ward, and David H Mathews. Deep learning models for RNA secondary structure prediction (probably) do not generalize across families. *Bioinformatics*, 38(16):3892–3899, June 2022.
- [65] Zhen Tan, Yinghan Fu, Gaurav Sharma, and David H. Mathews. TurboFold II: RNA structural alignment and secondary structure prediction informed by multiple homologs. *Nucleic Acids Research*, 45(20):11570–11581, September 2017.
- [66] Serbulent Unsal, Heval Atas, Muammer Albayrak, Kemal Turhan, Aybar C Acar, and Tunca Doğan. Learning functional properties of proteins with language models. *Nature Machine Intelligence*, 4(3):227–245, 2022.
- [67] Quentin Vicens and Jeffrey S. Kieft. Thoughts on how to think (and talk) about RNA structure. *Proceedings of the National Academy of Sciences*, 119(17), 2022.
- [68] R. Vitale, L. A. Bugnon, E. Fenoy, D. H. Milone, and G. Stegmayer. Evaluating large language models for annotating proteins. *Briefings in Bioinformatics*, 25(3):1–12, 2024.
- [69] Sarah von Löhneysen, Thomas Spicher, Yuliia Varenky, Hua-Ting Yao, Ronny Lorenz, Ivo Hofacker, and Peter F. Stadler. *Phylogenetic Information as Soft Constraints in RNA Secondary Structure Prediction*, page 267–279. Springer Nature Singapore, 2023.
- [70] Ning Wang, Jiang Bian, Yuchen Li, Xuhong Li, Shahid Mumtaz, Linghe Kong, and Haoyi Xiong. Multi-purpose RNA language modelling with motif-aware pretraining and type-guided fine-tuning. *Nature Machine Intelligence*, 2024.

- [71] Xi Wang, Ruichu Gu, Zhiyuan Chen, Yongge Li, Xiaohong Ji, Guolin Ke, and Han Wen. UNI-RNA: Universal pre-trained models revolutionize RNA research. *bioRxiv*, pages 1–10, 2023.
- [72] Hannah K. Wayment-Steele, Wipapat Kladwang, Alexandra I. Strom, Jeehyung Lee, Adrien Treuille, Alex Becka, and Rhiju Das. RNA secondary structure packages evaluated and improved by high-throughput experiments. *Nature Methods*, 19(10):1234–1242, 2022.
- [73] Sebastian Will, Kristin Reiche, Ivo L Hofacker, Peter F Stadler, and Rolf Backofen. Inferring noncoding rna families and classes by means of genome-scale structure-based clustering. *PLoS Computational Biology*, 3(4):e65, April 2007.
- [74] Run-Wen Yao, Yang Wang, and Ling-Ling Chen. Cellular functions of long noncoding rnas. *Nature Cell Biology*, 21(5):542–551, 2019.
- [75] Weijie Yin, Zhaoyu Zhang, Liang He, Rui Jiang, Shuo Zhang, Gan Liu, Xuegong Zhang, Tao Qin, and Zhen Xie. ERNIE-RNA: An RNA language model with structure-enhanced representations. *arXiv*, 1(1):1–10, 2024.
- [76] He Zhang, Liang Zhang, David H Mathews, and Liang Huang. LinearPartition: linear-time approximation of RNA folding partition function and base-pairing probabilities. *Bioinformatics*, 36(Supplement\_1):i258–i267, July 2020.
- [77] Jinsong Zhang, Yuhan Fei, Lei Sun, and Qiangfeng Cliff Zhang. Advances and opportunities in RNA structure experimental determination and computational modeling. *Nature Methods*, 19(10):1193–1207, 2022.
- [78] Yikun Zhang and et al. Multiple sequence alignment-based RNA language model and its application to structural inference. *Nucleic Acids Research*, 52(1):e3–e13, 2023.
- [79] Zhihan Zhou, Yanrong Ji, Weijian Li, Pratik Dutta, Ramana Davuluri, and Han Liu. Dnabert-2: Efficient foundation model and benchmark for multi-species genome, 2023.

## Funding

This work was supported by Argentine National Scientific and Technical Research Council (CONICET), ANPCyT (PICT 2022–0086) and UNL (CAI+D 2020 115). We also acknowledge the support of NVIDIA Corporation for the donation of GPU used for this research.

## Data availability

Curated benchmark datasets of increasing complexity are available in the repository: <https://github.com/sinc-lab/rna-llm-folding/tree/main/data>.  
 Moreover, all the embeddings generated in this study are available via Zenodo at: <https://doi.org/10.5281/zenodo.13821093>.  
 The source code to reproduce all the experiments and results can be found in: <https://github.com/sinc-lab/rna-llm-folding/>.